Magnetic Fields and the Cosmos

In honour of Jan Kuijpers' 65^{th} Solar revolution

Magenetic fields in Radio Pulsars

Janusz Gil & George Melikidze

Kepler Astronomical Institute
University of Zielona Góra, Poland

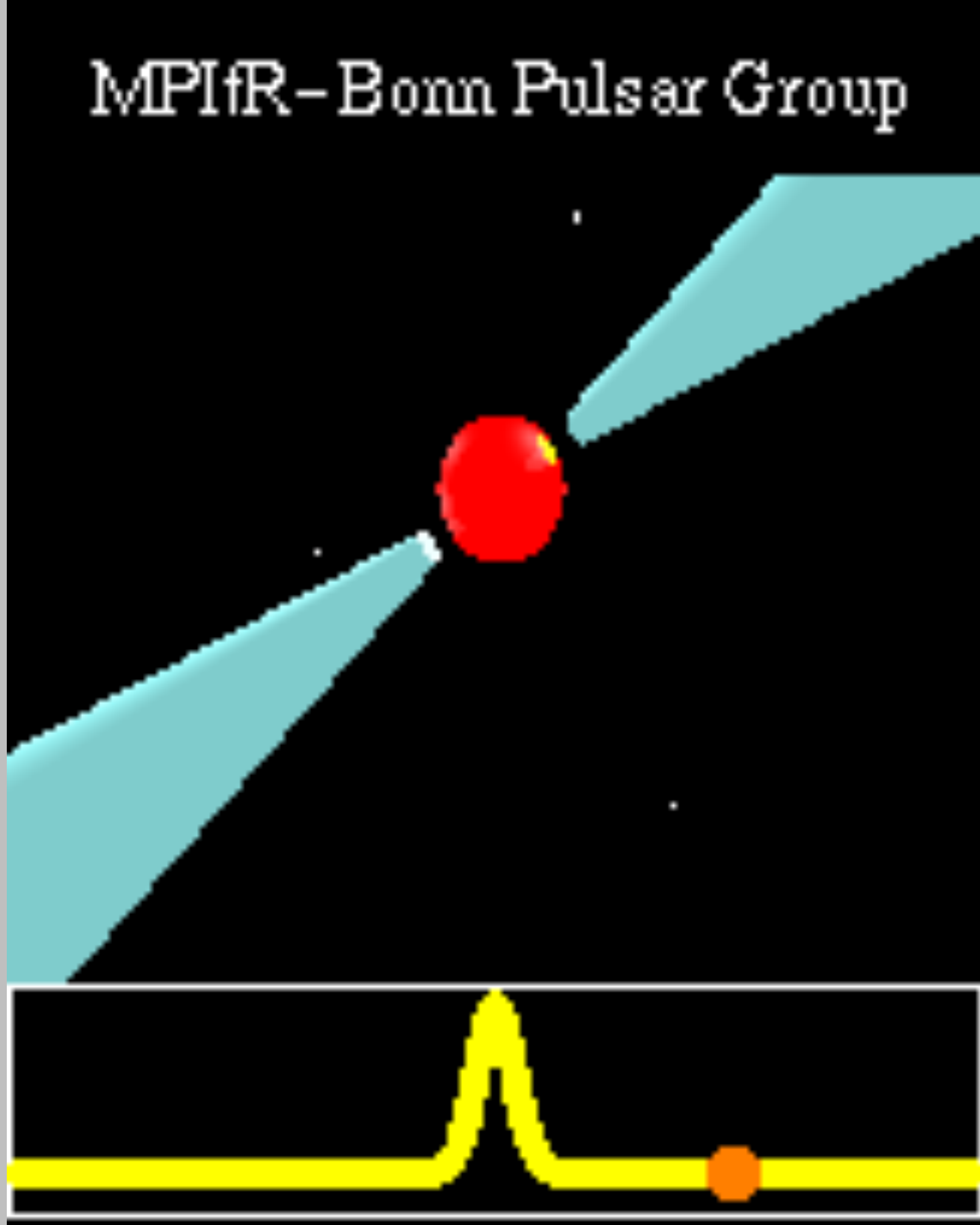
MPIfR - Bonn Pulsar Group

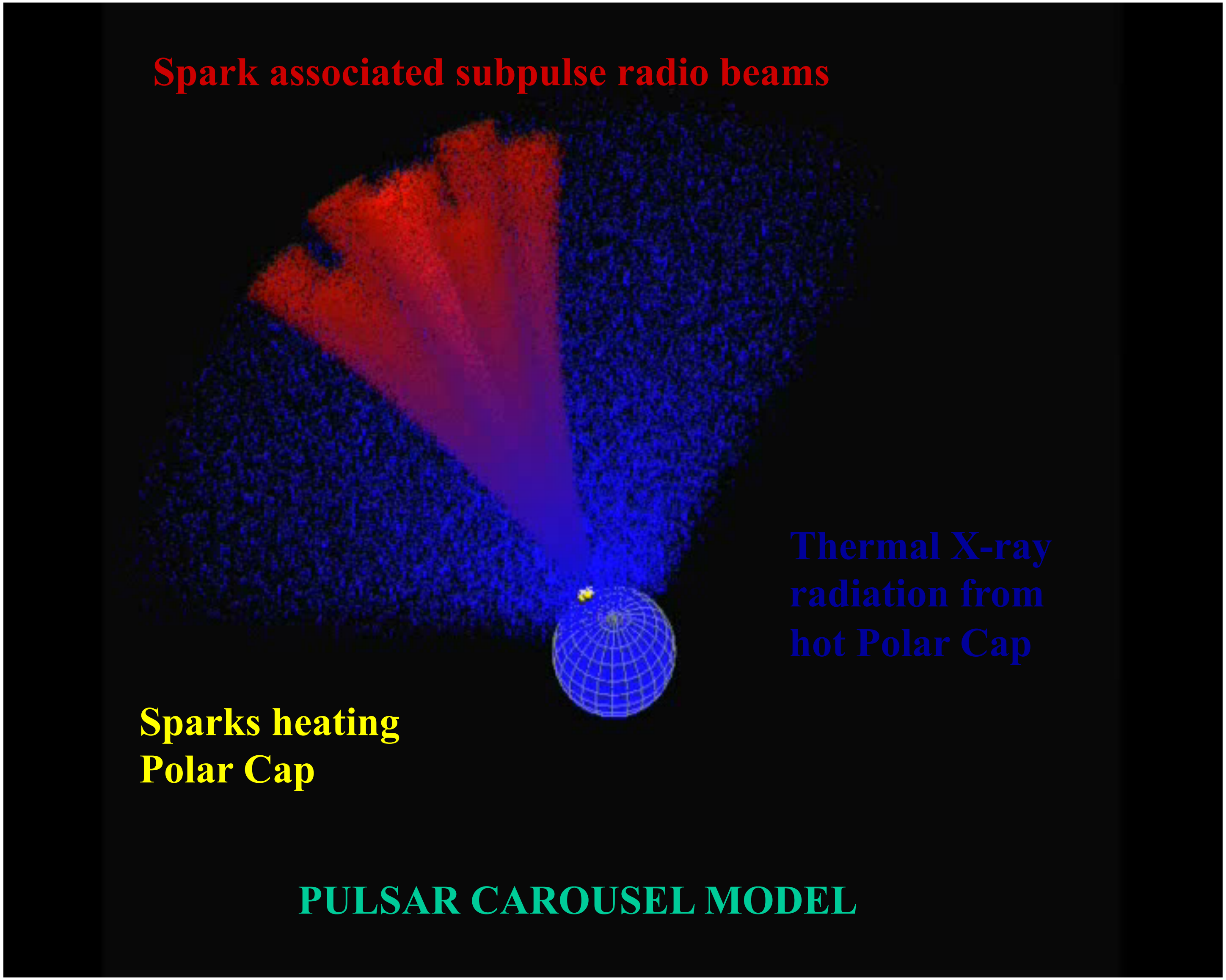
Spark associated subpulse radio beams
Thermal X-ray
radiation from
hot Polar Cap
Sparks heating
Polar Cap
PULSAR CAROUSEL MODEL

Co-rotating magnetosphere

$$E_c = -(\Omega \times r / c) \times B_s$$

Force-free magnetosphere

$$E_c \cdot B_s = 0$$

$$\Delta V_{||} = 0$$

No acceleration along *B*

GJ69, RS75

$$\rho_c = (1/2\pi)\, divE_c =$$

$$= -\Omega \cdot B_s /(2\pi c) = \pm B_s / cP$$

Co-rotating charge density

$$\upsilon_{cor} = c(E_c \times B_s) / B^2 = cE_c / B_s$$

Linear co-rotation velocity

$$\upsilon_{dr} = c(\Delta E_c \times B_s) / B^2 = c\Delta E_c / B_s$$

Non-corotation

Pulsar radiation requiers acceleration of charged particles along magnetic field lines -> electric field along field lines -> NON-CORROTATION

Evidence of NON-CORROTATION should be clearly present in pulsar data

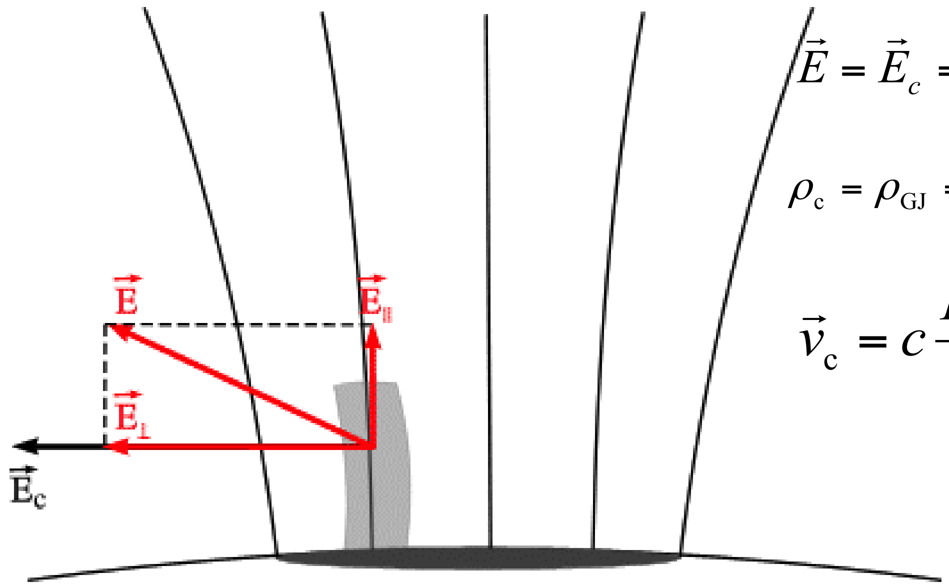

$$\vec{E} = \vec{E}_c = \frac{1}{c}\vec{B}_s \times \left(\vec{\Omega} \times \vec{r}\right)$$

$$\rho_c = \rho_{GJ} = -\frac{\left(\vec{\Omega} \cdot \vec{B}_c\right)}{cP}$$

$$\vec{v}_c = c\frac{\vec{E}_c \times \vec{B}_s}{B_s^2}$$

$$\vec{E} = \vec{E}_{\parallel} + \vec{E}_{\perp} \qquad \Delta\vec{E}_{\perp} = \vec{E}_c - \vec{E}_{\perp}$$

$$\rho_c = (1-\eta)\rho_{GJ}; \quad \eta << 1$$

Non-corotation

$$\vec{v}_{df} = c\frac{\Delta\vec{E}_{\perp} \times \vec{B}_s}{B_s^2}$$

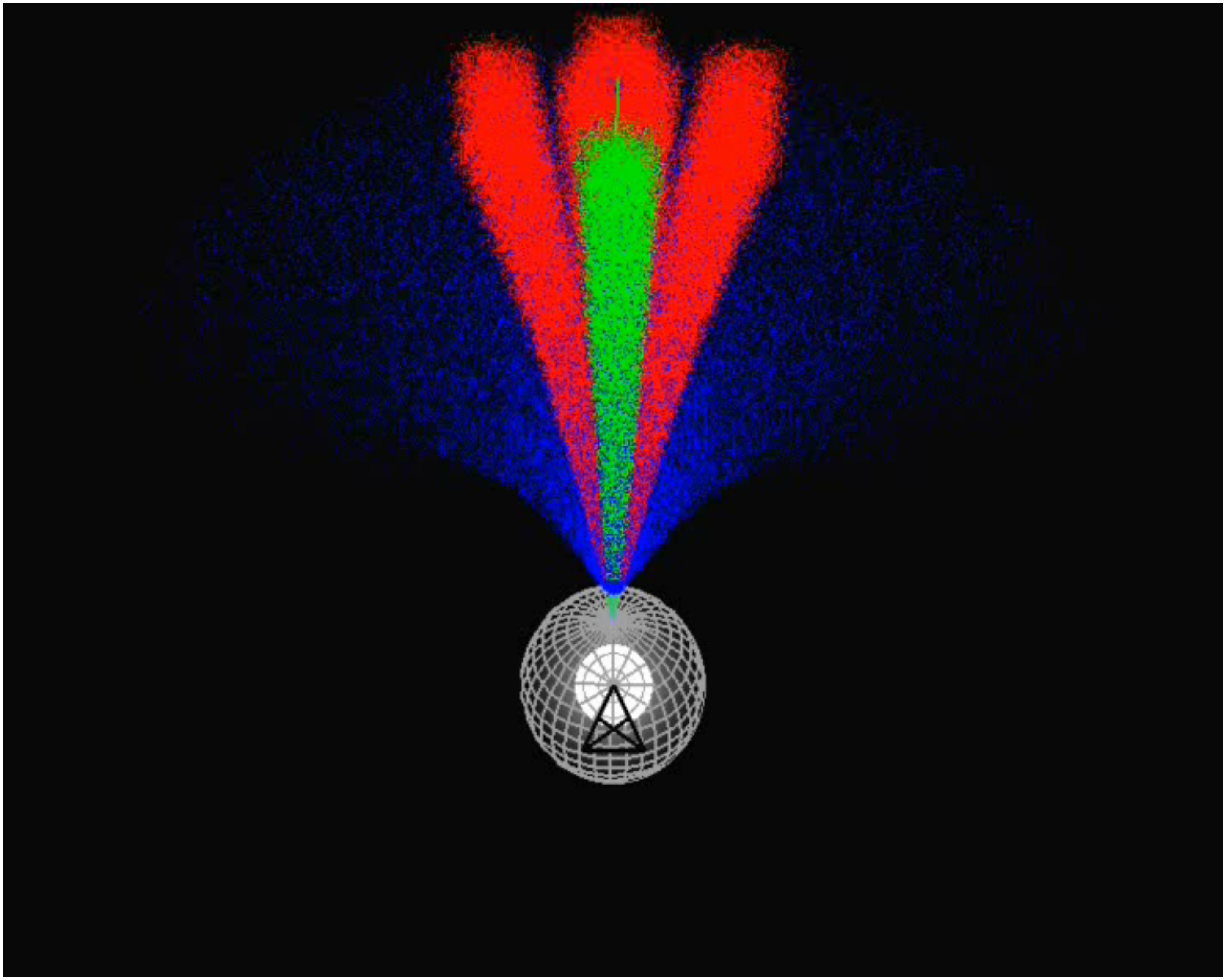

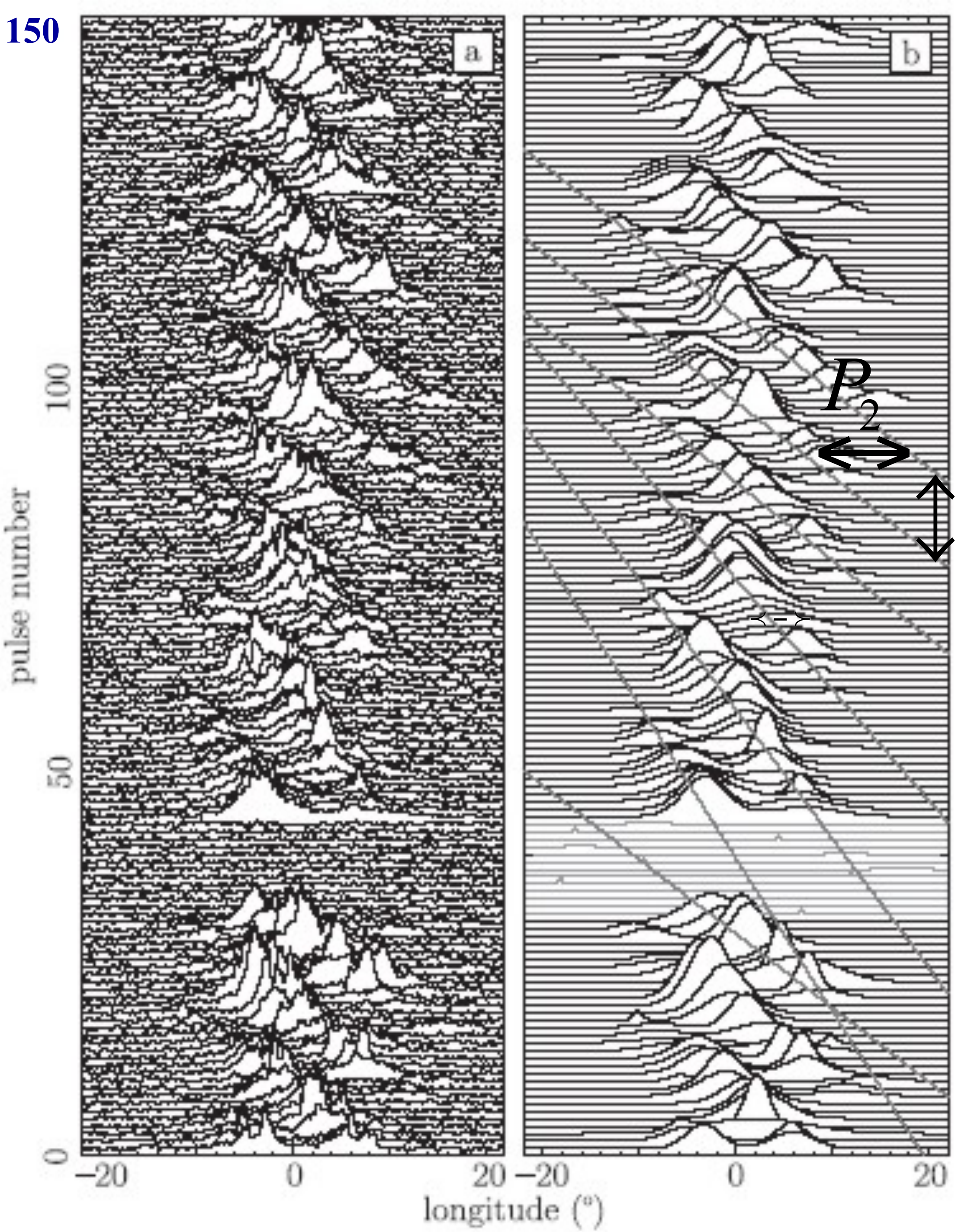

PSR B0809+74

Line-of-sight (l-of-s) grazing
the overall pulsar beam

Apparent subpulse drift-bands

$P_3 \approx 11P$

Modulation of intensity along
drift-bands consistent with
carousel model

that is

Sub-beams seem to continue
to circulate beyond
the observed pulse-window

(after van Leuven, Stappers et al..)

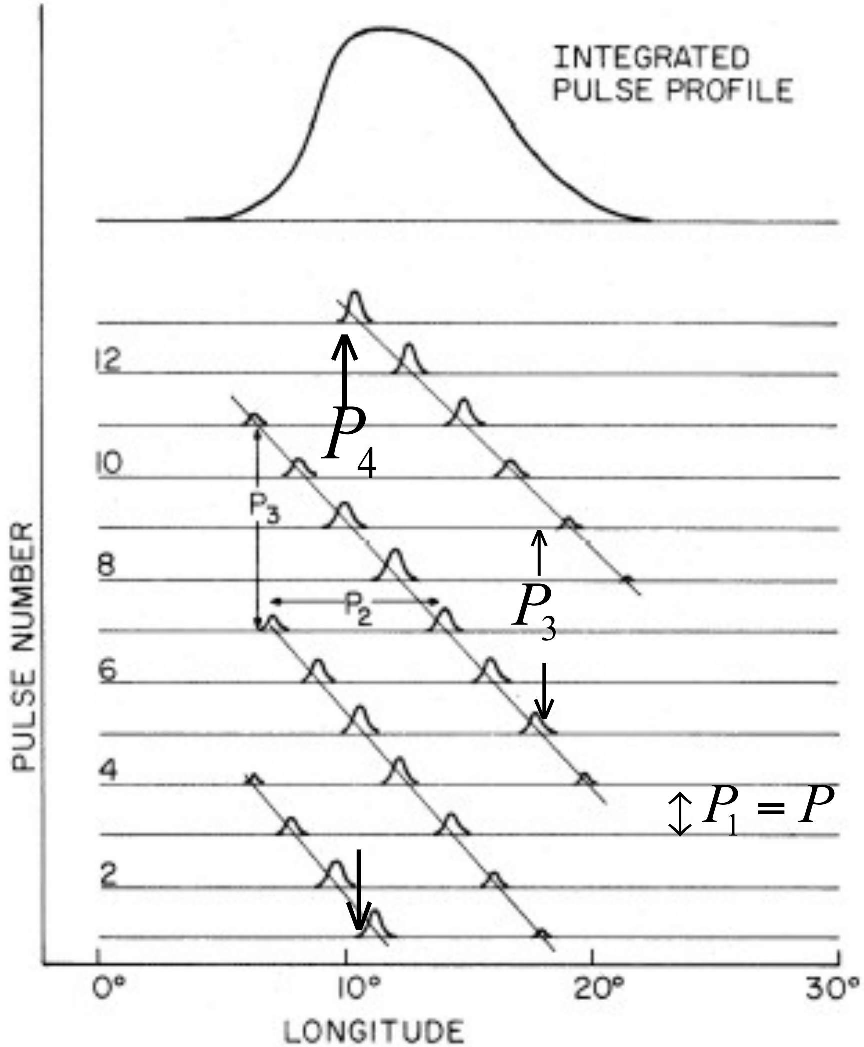

FIG. 5.—Schematic (after Backer 1973) of integrated pulse profile, arrival times of individual pulses, and definition of P_2, P_3 for those pulsars showing the "drifting subpulse" phenomenon. Arrival times of individual pulses are given in terms of a longitude for which 360° corresponds to the full pulsar period.

Ruderman & Sutherland 1975

$$P_1, P_2, P_3, P_4$$

Apparent drift rate $D = P_2 / P_3$

P_2 **distance between driftbands in longitude**

P_3 **distance between driftbands in** P_1

Intrinsic drift rate $P_4 = P_3 N$

N **number of rotating sub-beams**

P_4 **distance between the same driftbands**

P_4 **time interval to complete one rotation around the pole**

very difficult to measure, only 8 cases known !!!

PSR B0943+10

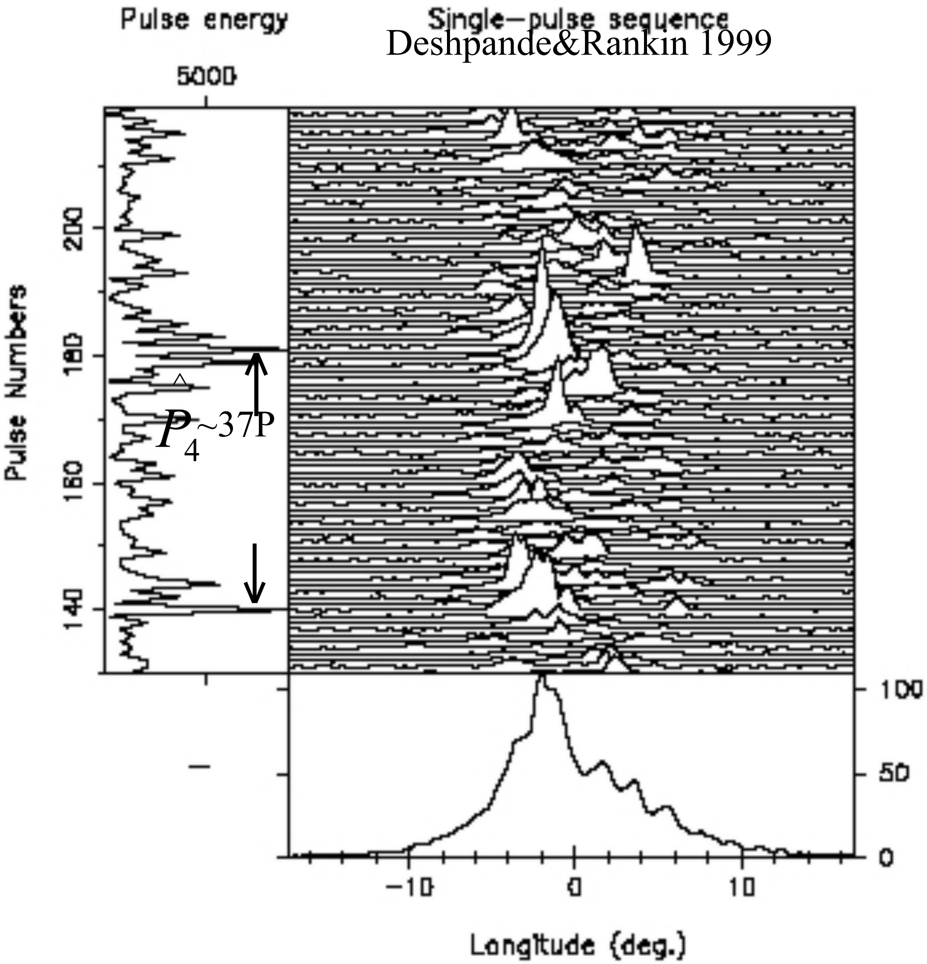

$$P_1 = 1.089s$$

$$P_3 = 1.87P$$ primary

$$P_3' = 2.15P$$ aliased

$$P_4 = 37.35P$$

Number of sub-beams circulating around B

$$N = P_4 / P_3 = 20$$

PSR B0943+10

Deshpande & Rankin 1999, 2001
Asgekar & Deshpande 2001

Phased-resolved fluctuation spectrum

Fourier transform

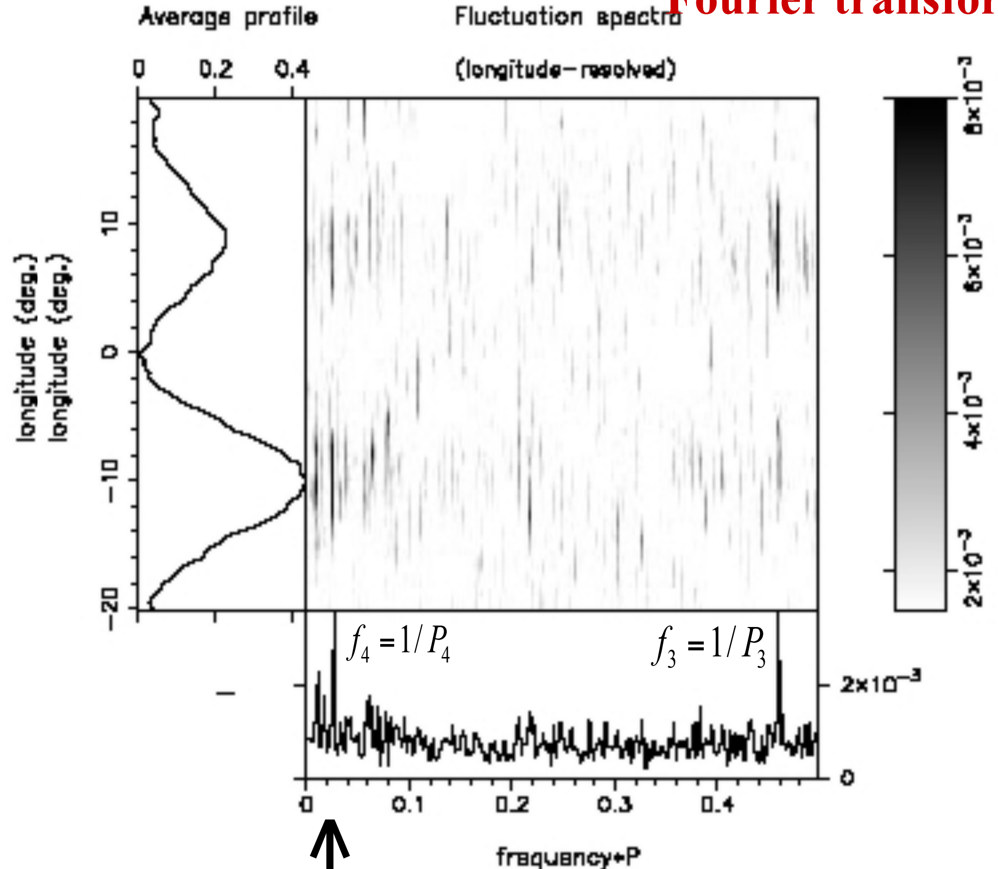

$$P_4 = 37.35\, P_1 = 41\,\mathrm{s}.$$

1/37=0.027

1/1.87

Spectral analysis fully consistent with „carousel model". Sub-beams continue to circulate around the beam axis beyond the pulse-window and reapear after the period needed to complete one full circulation around the magnetic axis

$$N = P_4 / P_3 = \frac{37.35}{1.87} = 19.97 \sim 20$$

20 sub-beams

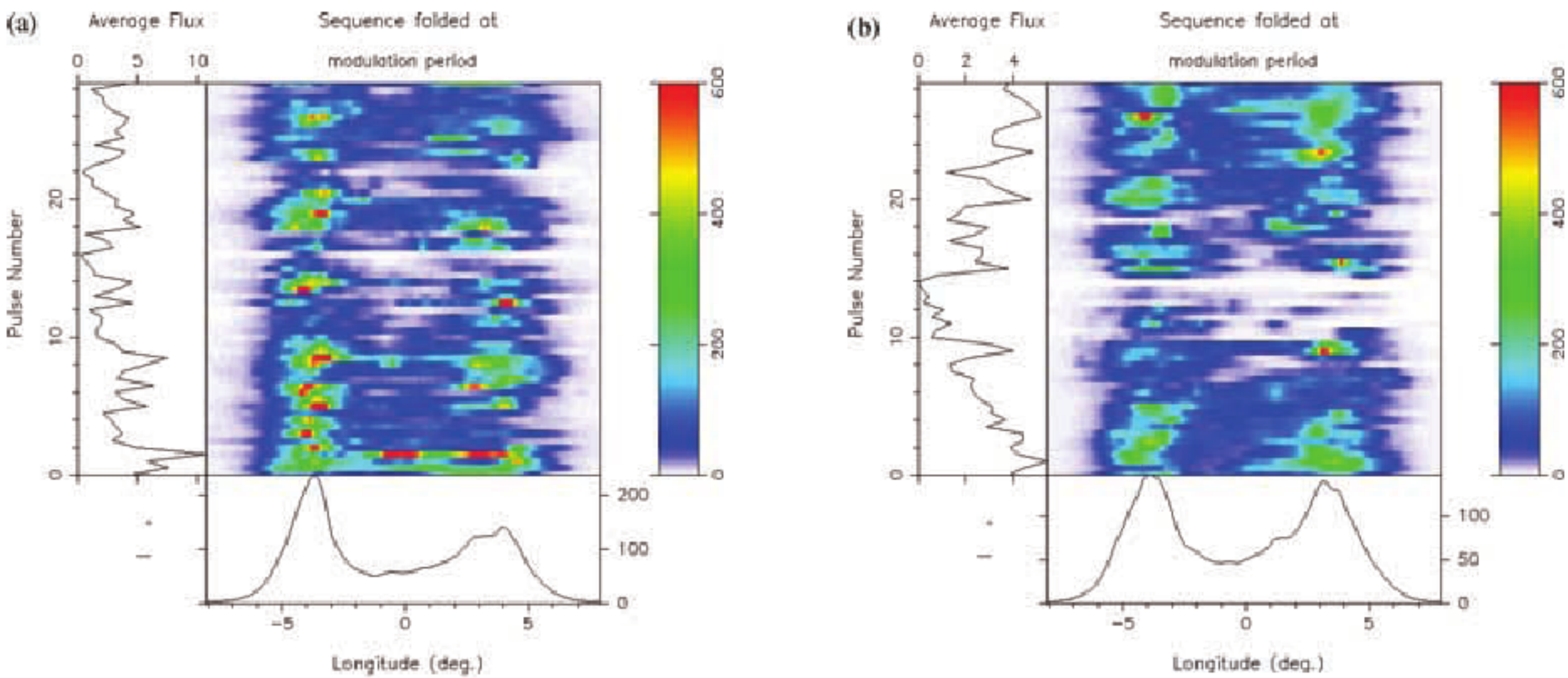

Figure 7. Typical 113-pulse intervals of observation A (in Table 1) folded at the local $28.44P_1$ putative value of $\hat{P}_3$. Each display represents the average of four such intervals. Note that both folded PSs show one or more 'null zones' where the intensity is negligible as well as maxima that are three to five times larger than the average.

B1133+16

Rankin et al. 2007

B1133+16

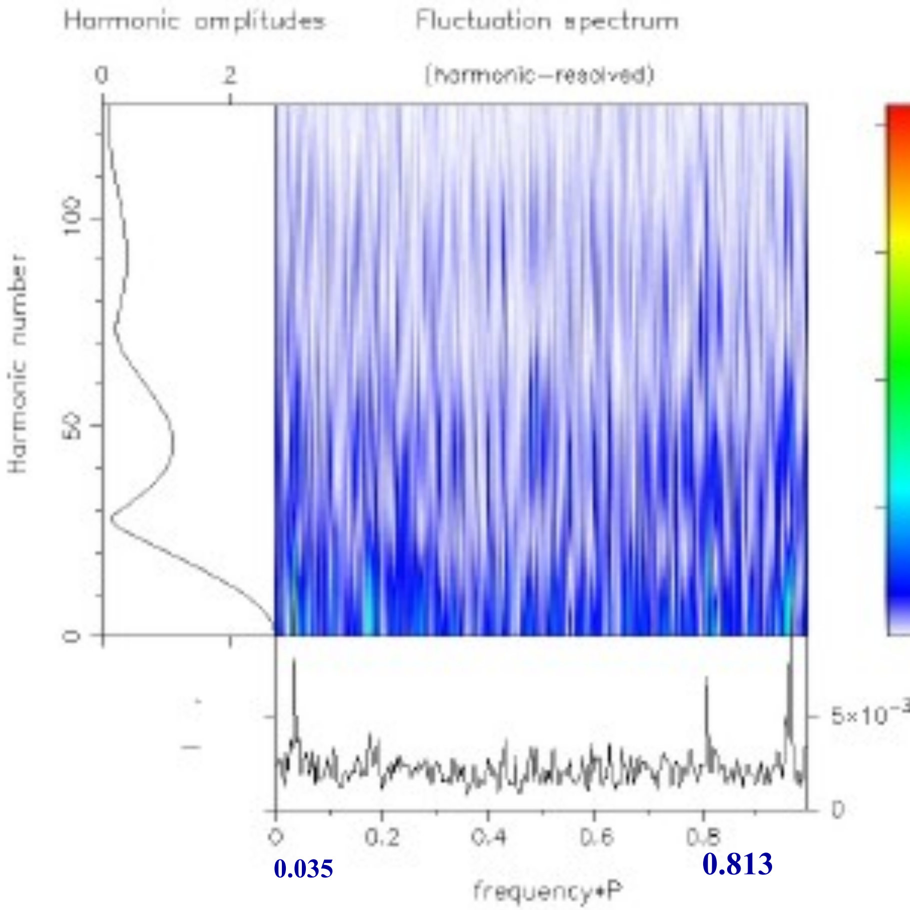

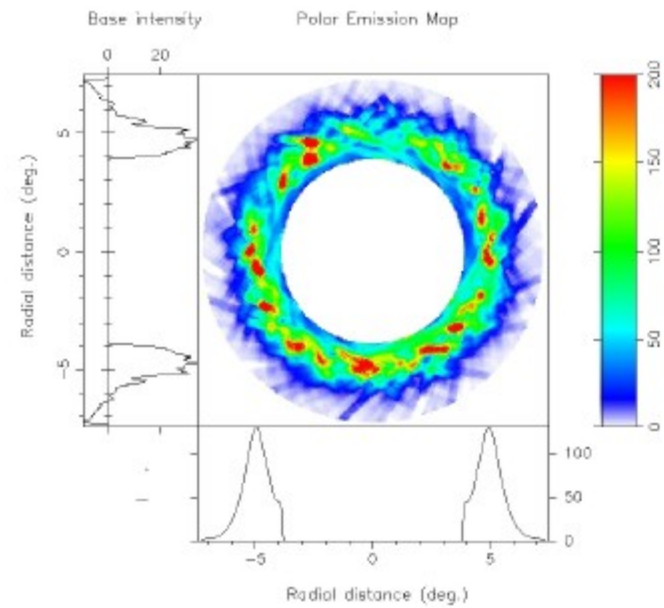

Figure A2. Polar map constructed using pulses 242-504 of the A PS. Here, $\hat{P}_3$ was determined to be 28.44 P_1, so the average of 7 carousel rotations is depicted. The magnetic axis is at the centre of the diagram, the "closer" rotational axis is upward, and (assuming a positive or equatorward traverse) the sightline track sweeps through the lower part of the pattern. Here, the star would rotate clockwise, causing the sightline to cut the counter-clockwise-rotating subbeam pattern from right to left; see DR01 for further details. The side panels give the "base" function (which has not been subtracted from the map), and the lower panel shows the radial form of the average beam pattern.

$$P_4 = 28.44 P_1 \qquad N = P_4 / P_3 = 22.991 \pm 0.01 = 23$$

$$P_3 = (1.237 \pm 0.011) P_1$$

23 sub-beams

Rankin et al. 2007
325 MHz Arecibo

8.35 GHz
Effelsberg
data

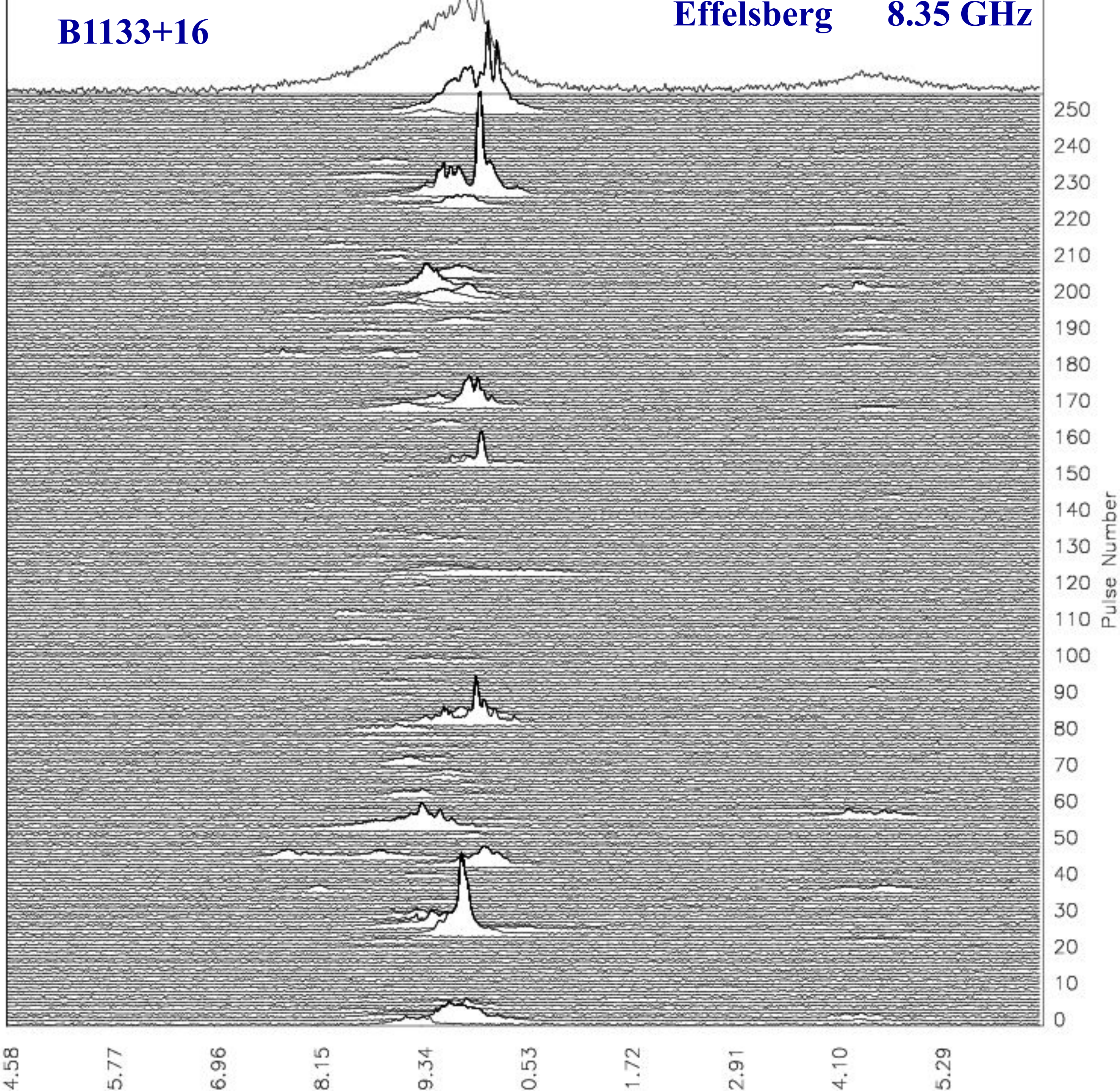

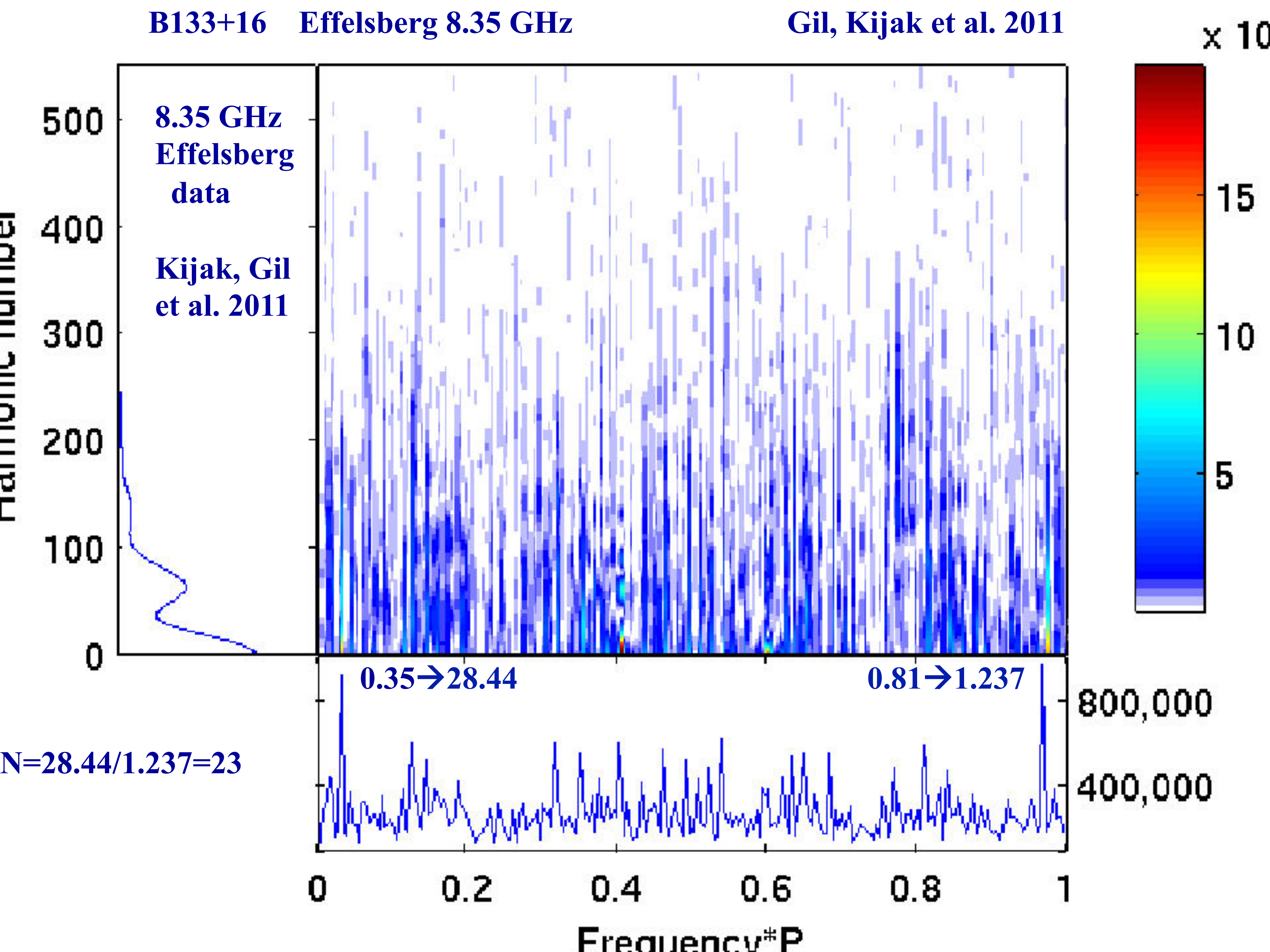
B133+16 Effelsberg 8.35 GHz
Gil, Kijak et al. 2011
8.35 GHz
Effelsberg
data
Kijak, Gil
et al. 2011
Harmonic number
500
400
300
200
100
0
x 10
15
10
5
0.35→28.44
0.81→1.237
N=28.44/1.237=23
800,000
400,000
0
0.2
0.4
0.6
0.8
1
Frequency*P

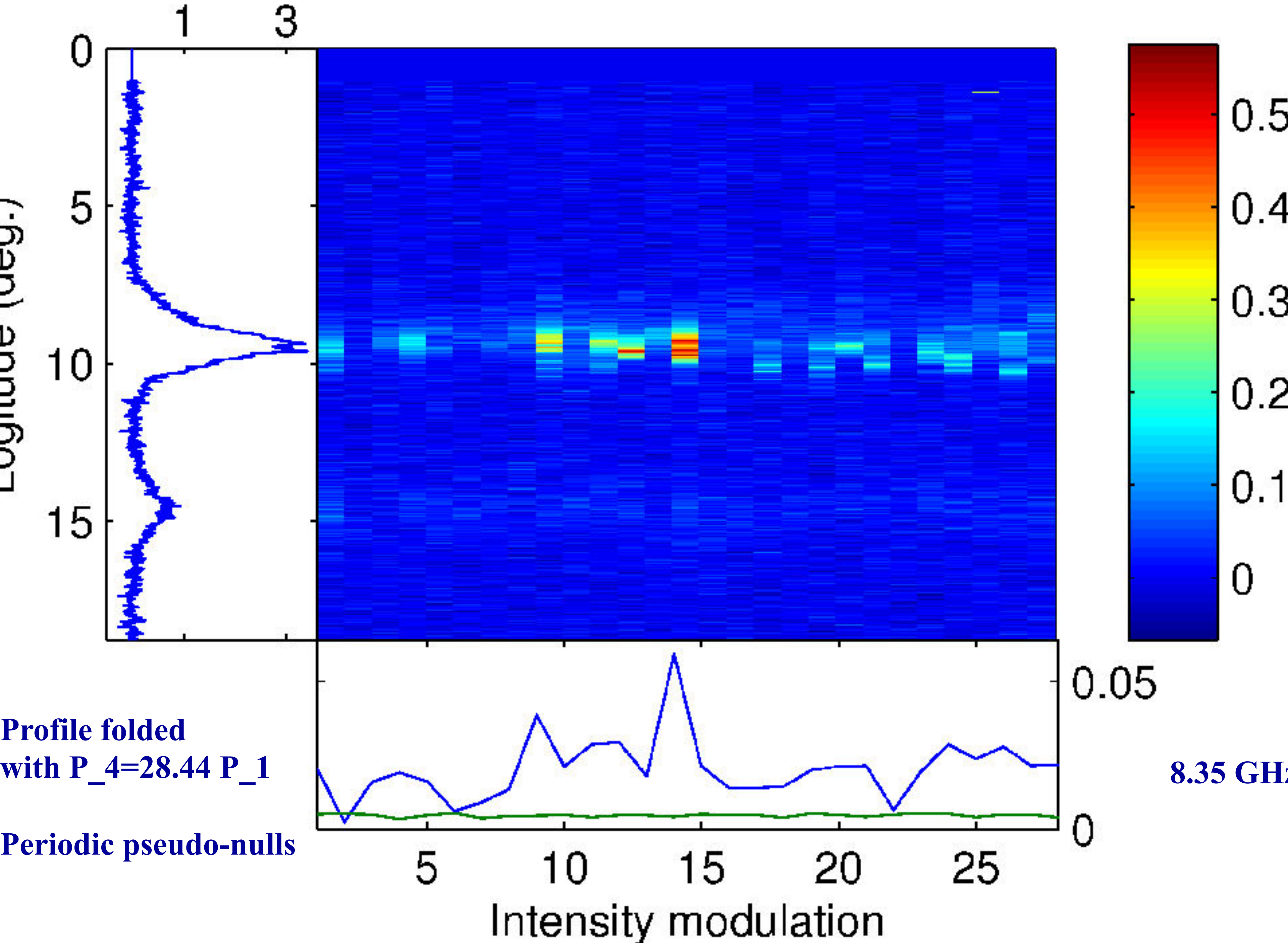

Profile folded with P_4=28.44 P_1

Periodic pseudo-nulls

8.35 GHz

In radio band very erratic pulsar B0656+14

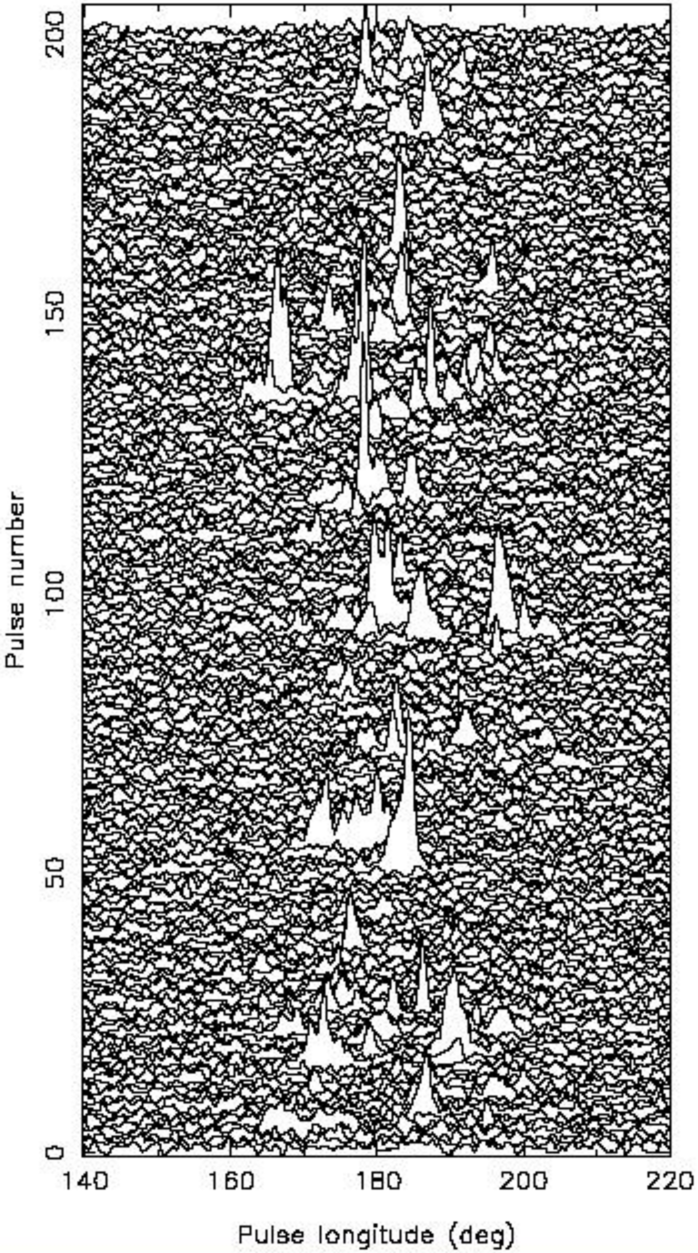

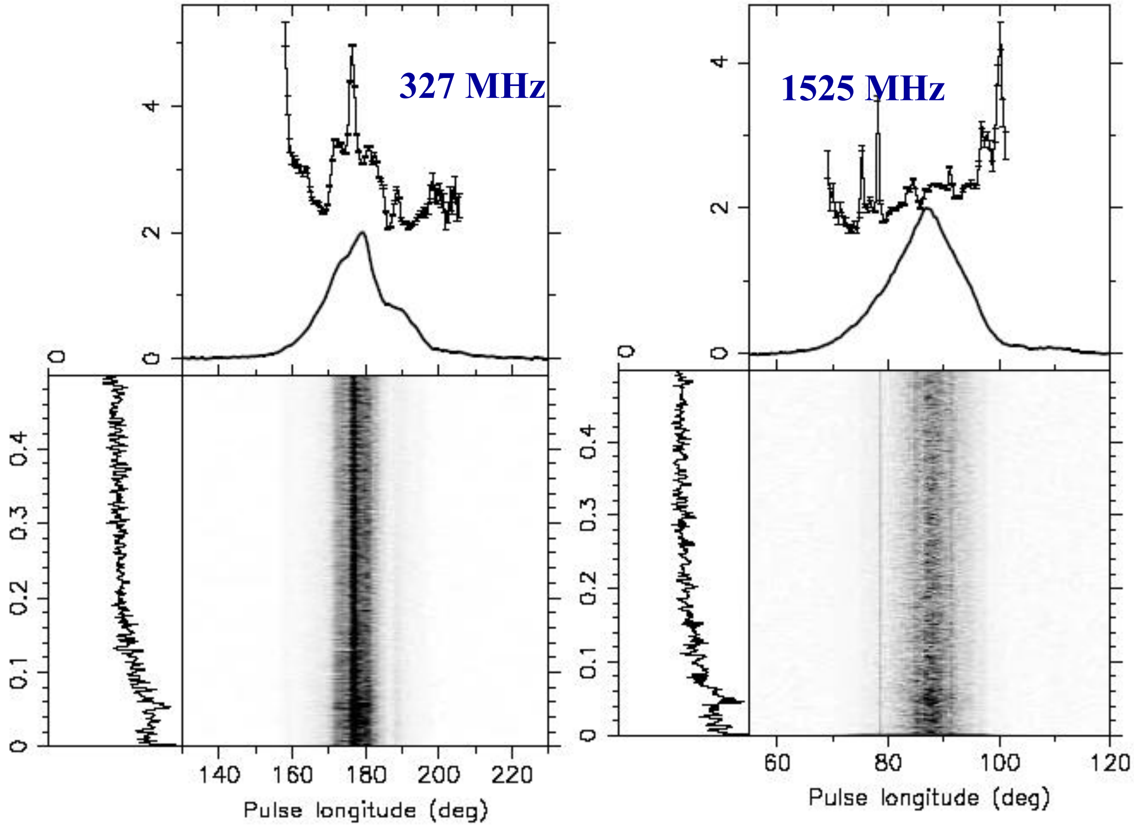

Clear intesity modulation feature at 20 P in the fluctuation spetrum

$$P_4 = 20P$$

Weltevrede et al.. 2006

Q-mode or spiky mode

$$L_x = 570 \times 10^{28} erg / s$$

Partially Screened Gap (PSG model)

1. Positive charges cannot be supplied at the rate that would compensate the inertial outflow through the light cylinder. As a result, significant potential drop develops above the polar.
2. Back-flow of electrons heats the surface to temperature above 10^6 K.
3. Thermal ejection of iron ions causes a partial screening of the acceleration potential drop.
4. Consequently, backflow heating decreases as well.
5. Thus heating leads to cooling – this is a classical thermostat.
6. Surface temperature T_s is thermostatically regulated to retain its value close to critical temperature T_i above which thermal ion flow reaches co-rotation limited level (Goldreich-Julian charge density)
7. According to calculations of cohesive energy by Medin-Lai (2007), this can occur if the surface magnetic field is close to 10^{14} G. In majority of radio pulsars this has to be highly non-dipolar crust anchored field.

More details on PSG model in G. Melikidze's talk

First explanation of drifting subpulses – Sparking Inner Gap model (RS75)
Non-corotation potential drop too high > 10^12 V
too fast a subpulse drift as compared with observations
too hot polar cap (backflow bombardment) –10^7 K not observed in X-rays

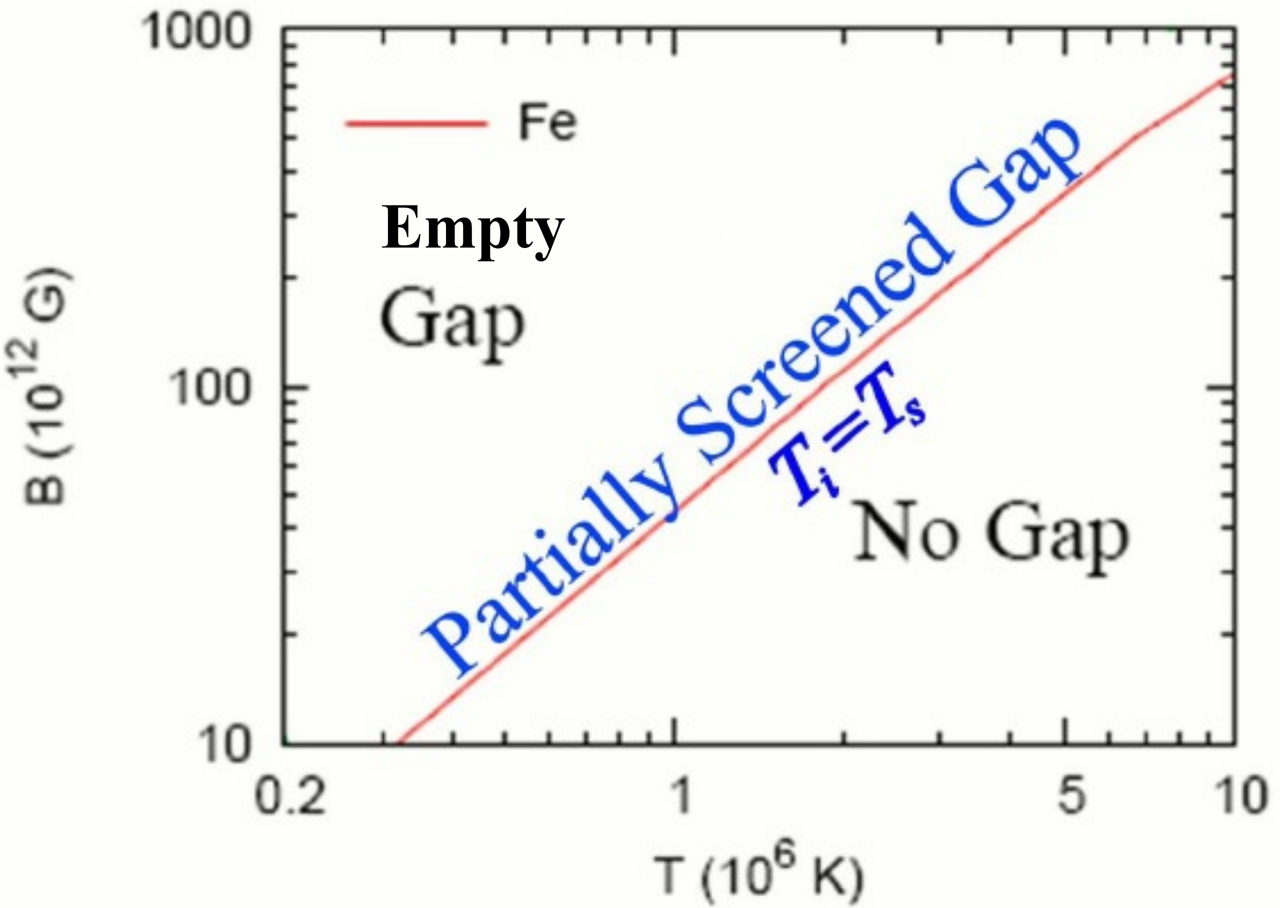

Recent calculations indicate that the cohesive energy of condensed matter increases with magnetic field strength (Medin & Lai 2007, MNRAS)

Partialy Screened Gap (PSG) model

Gil, Melikidze & Geppert 2003 , A&A 407,315

Electron-positron plasma created in sparks co-exists with thermionic flow caused by back-flow bombardment

$$\boxed{\rho_{\pm} + \rho_{th} = \rho_{GJ}}$$

Surface temperature of spark-heated polar cap

ε **- cohesive energy**

$$T_s \geq 10^6 \ K$$

$$T_s \leq T_i$$

Iron Ion critical temperature (Jones 1986, Medin & Lai 2007)

$$T_i = \varepsilon / 30k = (7 \times 10^4 \ K)(B_s / 10^{12} \ G)^{0.7}$$

$$B_s \sim 10^{13-14} \ G$$

above this T there is maximum thermionic flow from the PC surface with GJ density (no sparking)

$$\eta = 1 - \rho_{th} / \rho_{GJ} = 1 - \exp[30(1 - T_i / T_s)]$$

Screening factor determined by thermoregulation of PSG

Thermoregulation of PSG

Backflowing bombardment associated with spark plasma development heats the PC surface to temperatures lower than critical temperature (above which free thermal out-flow from the surface).

$$L_b = A_p \sigma T_s^{\,4}$$

The higher the temperature the more intense thermionic emission, which in turn means more screening and less intense heating.

This thermolegulation should establish the quasi-steady state at temperature very close (but slightly lower) to the critical temperature

$$\boxed{T_s \cong T_i}$$

Possible interrelation between radio and X-ray signatures of drifting subpulses in pulsars

L_b **versus** P_4

Thermal (bolometric) luminosity from polar cap heated by sparks associated with (drifting) subpulses

$$L_b = \sigma T_s^4 A_{bol} = \sigma T_s^4 A_{pc} (B_d / B_s)$$

Tertiary (carousel) subpulse drift periodicity → circulation period of subpulse associated sparks

$$P_4 / P_1 \approx 2\pi r_p / \upsilon_d = 2 r_p / h\eta$$

Thermal X-ray luminosity from spark-heated polar cap

$$L_b = 2.5 \times 10^{31} \times (P_{-15} / P^3)(P_4 / P)^{-2} \quad erg/s$$

Efficiency of thermal radiation from hot PC

$$\boxed{L_b / \dot{E} = (0.63 / I_{45})(P_4 / P)^{-2}}$$

$$\dot{E} = I\Omega\dot{\Omega}$$

Spin-down power

Relationship between P_4 (radio observations) and BB luminosity L_b of thermal X-ray emission from the hot PC

$$I = I_{45} 10^{45} \, g \, cm^2$$

$$I_{45} = 1 \pm 0.15$$

Intensity of thermal BB radiation is correlated with plasma circulation rate

$$L_b / \dot{E} = (0.63 / I_{45})(P_4 / P)^{-2}$$

L_b - **Polar Cap heating rate due to** $\Delta E_{\|}$

P_4 - **Plasma circulation rate due to** $\Delta E_{\perp}$

$\Delta E_{\|} \sim \Delta E_{\perp}$ **Two components of the non-corotation electric field above the Polar Cap**

X-ray Multi Mirror (XMM) – Newton satelite telescope

One revolution on an excentric orbit around the Earth takes 48 hours – observations are not performed close to the Earth due to strong noise contamination

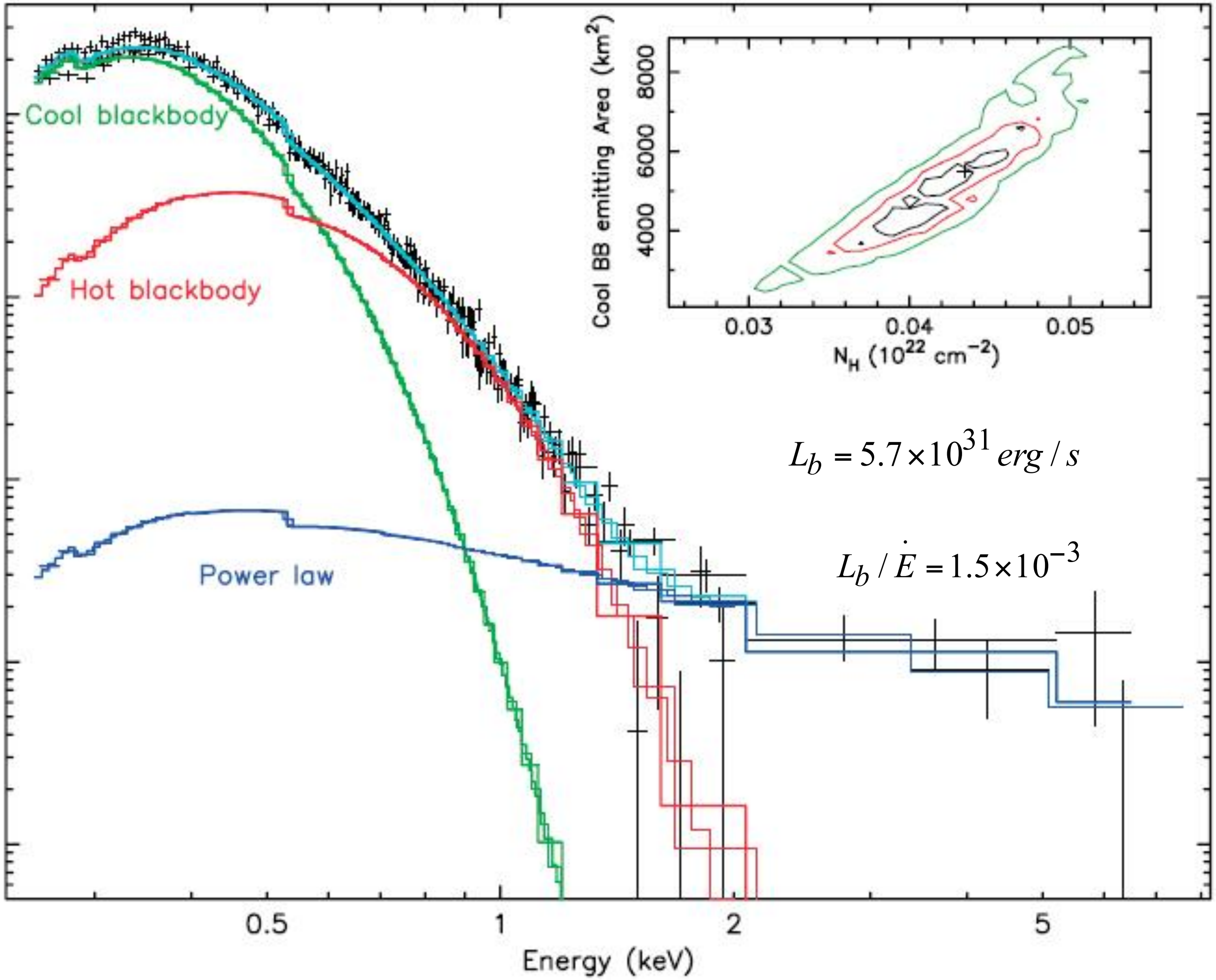

r PSR B0656+14. Data from pn (both small-window and fast-timing mode) and MOS1 are plotted (*black points*). Detailed values reported in Table 2.

Clear cut case
B0656+14

No question that hot blackbody (HBB) originates on the Polar Cap

Size of the HBB Emitting area much smaller than the canonical PC

PSR B0943+10

$$P = 1.0977\,\mathrm{s},\ \dot{P}_{-15} = 3.49$$

$$A_{pc} \approx 6\times10^4\,\mathrm{m}^2$$

$$A_{\mathrm{BB}} \approx 10^3\,\mathrm{m}^2$$

$$A_{pc} \approx 60\,A_{\mathrm{BB}}$$

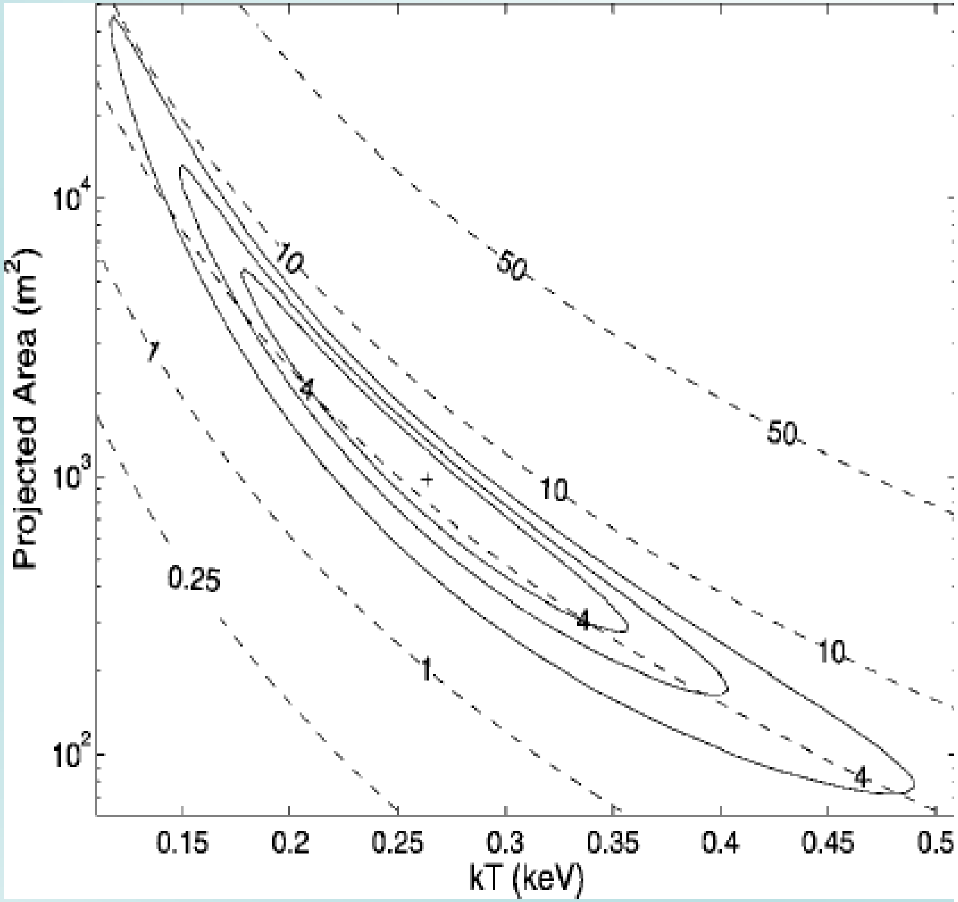

Confidence contours (68%, 90%, and 99%), computed for BB model fits to the spectrum of PSR B0943+10. (Zhang, Sanwal & Pavlov, ApJ, 624, L109, 2005)

PSR B1133+16

$$P = 1.188\,\mathrm{s},\ \dot{P}_{-15} = 3.73$$

$$A_{pc} \approx 5.5 \times 10^4\ \mathrm{m}^2$$

$$A_{\mathrm{BB}} \approx 5 \times 10^2\ \mathrm{m}^2$$

$$A_{pc} \approx 100\, A_{\mathrm{BB}}$$

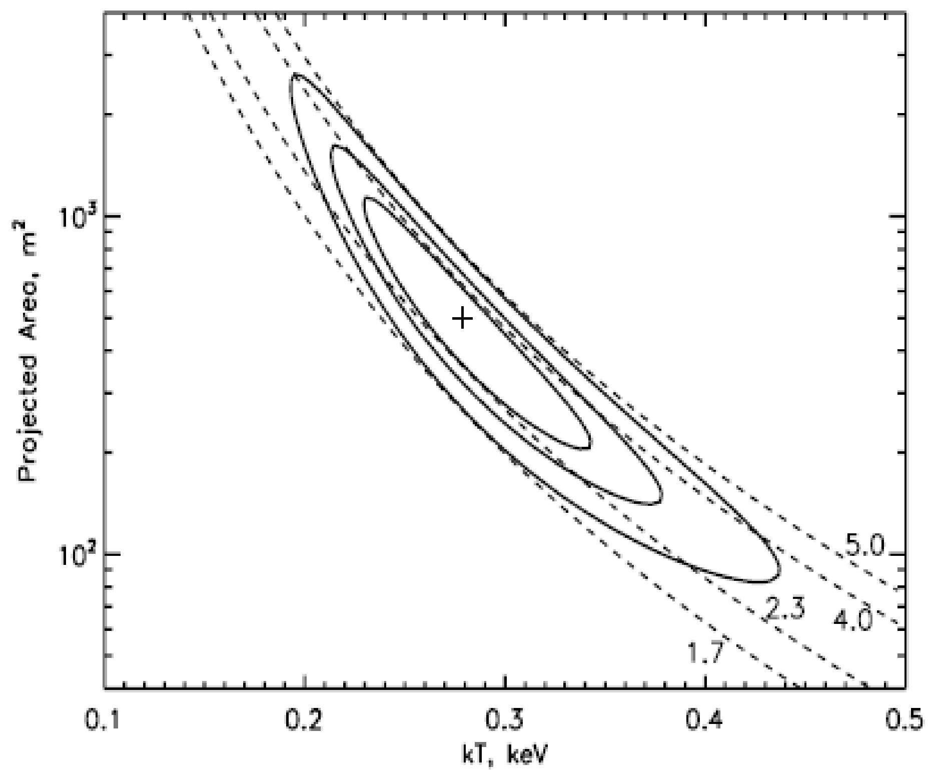

Confidence contours (68%, 90%, and 99%), computed for BB model fits to the spectrum of PSR B1133+16. (Kargaltsev, Pavlov & Garmire, ApJ, 636, 406, 2006)

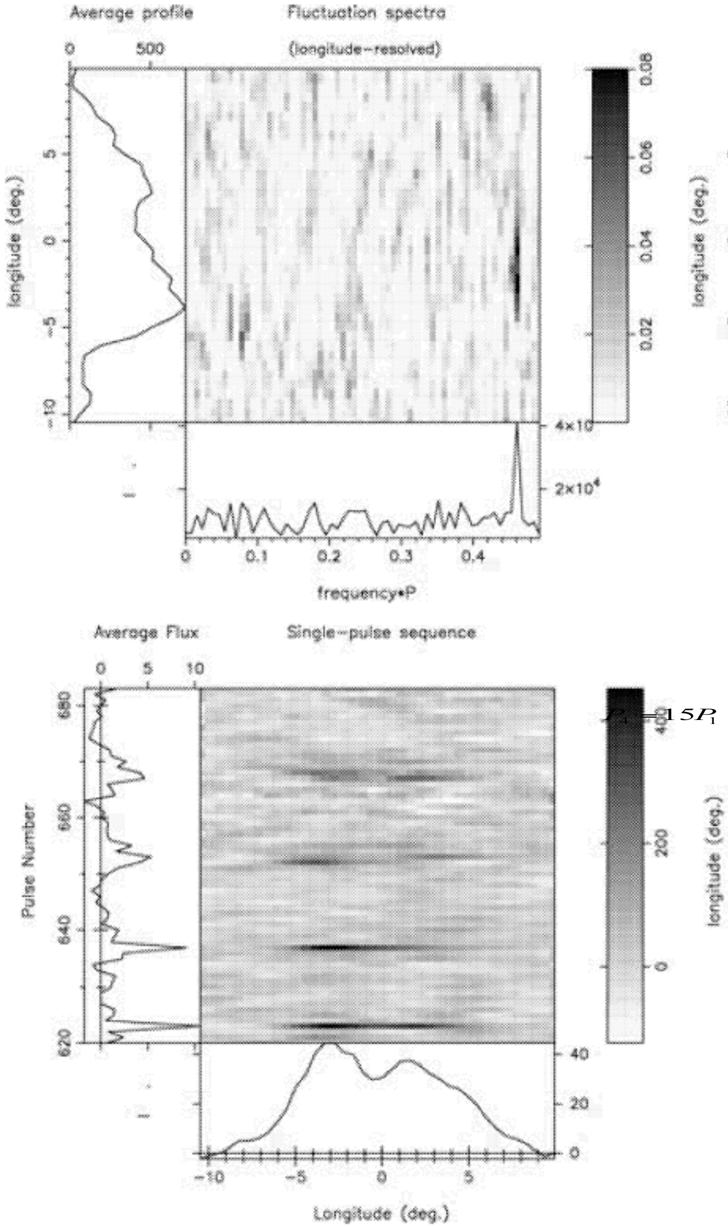

B0834+06

$f_3 = 0.46c/P_1$

$f_4 = (1/15)c/P_1$

$P_4 = 15P_1$

Figure 3. (Left) A 64-pulses long section of the C sequence shown in grey-scale; and (right) longitude-resolved spectrum of this section of the sequence. Note the strong feature at 0.07 c P_1^{-1} and the near absence of modulation feature at 0.46 c P_1^{-1}.

Asgekar & Deshpande 2005, MNRAS

Gil, Haberl, Melikidze 2008, ApJ 686,497

+ proposal $P_4 / P = 15$

+ data $P_4 / P = 30$

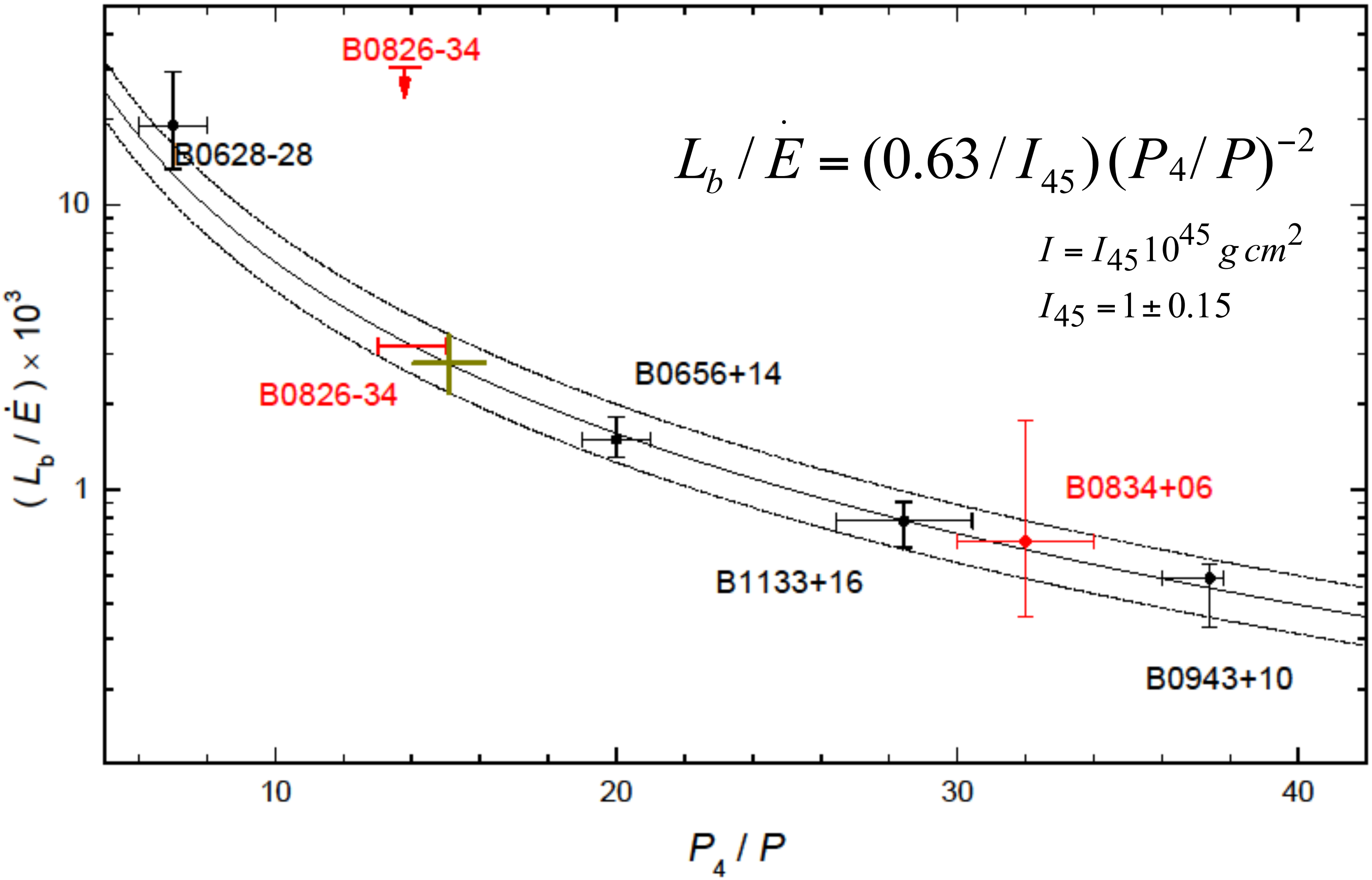

50 ks XMM

B0834+06

70 counts

$$L_b = (8.6^{+14.2}_{-4.4}) \times 10^{28}\ erg/s$$

$$T_s = (2.0^{+2.0}_{-0.9}) \times 10^{6}\ K$$

B0834+06

$$f_3 = (0.4609 \pm 0.0019)c / P_1$$

$$P_3 = (2.169 \pm 0.01)P_1$$

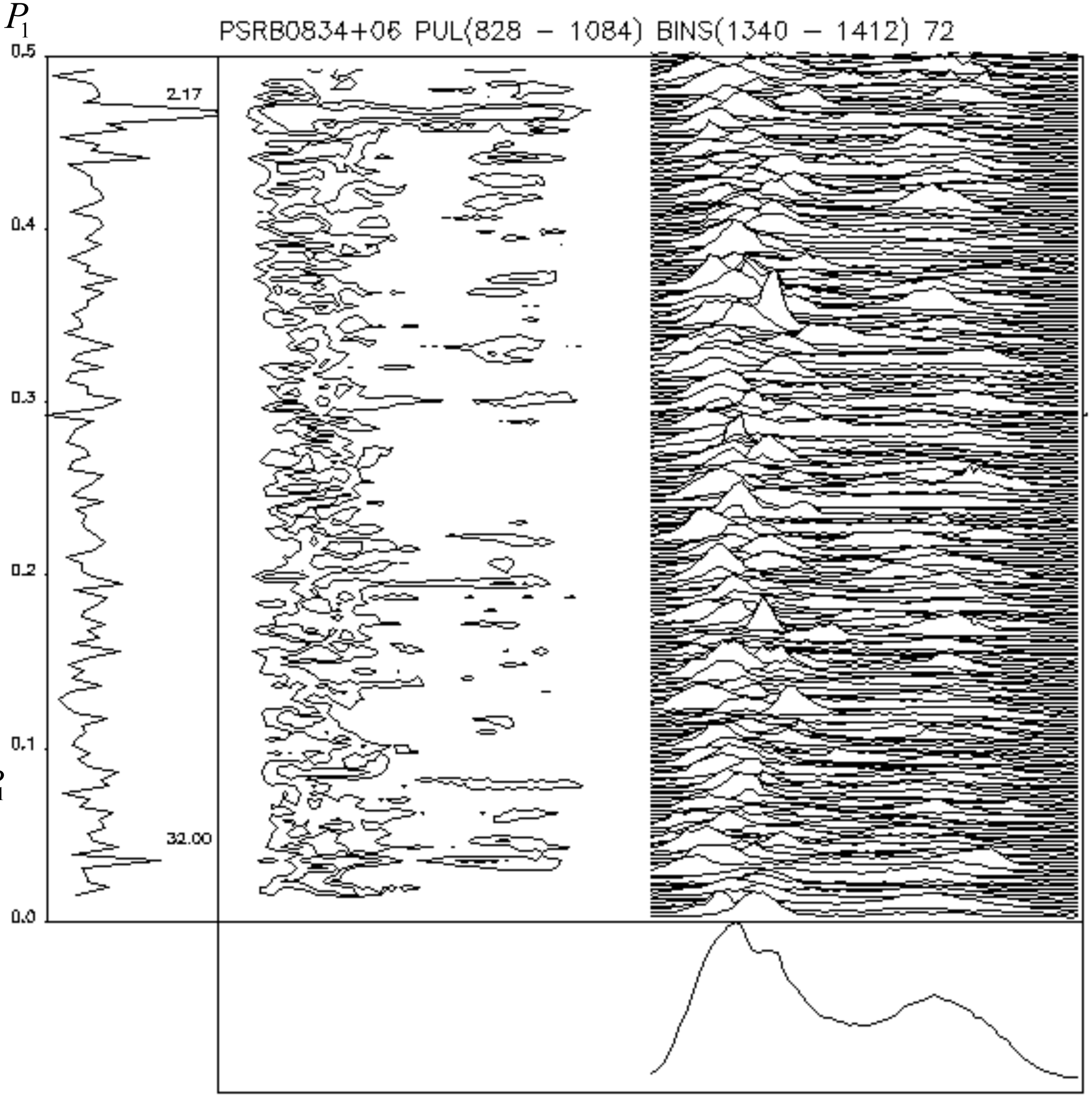

GMRT
India

$$f_4 = (0.0312 \pm 0.0019)c / P_1$$

$$P_4 = (32 \pm 2)P_1$$

Gil, Mitra, Sendyk (2010)

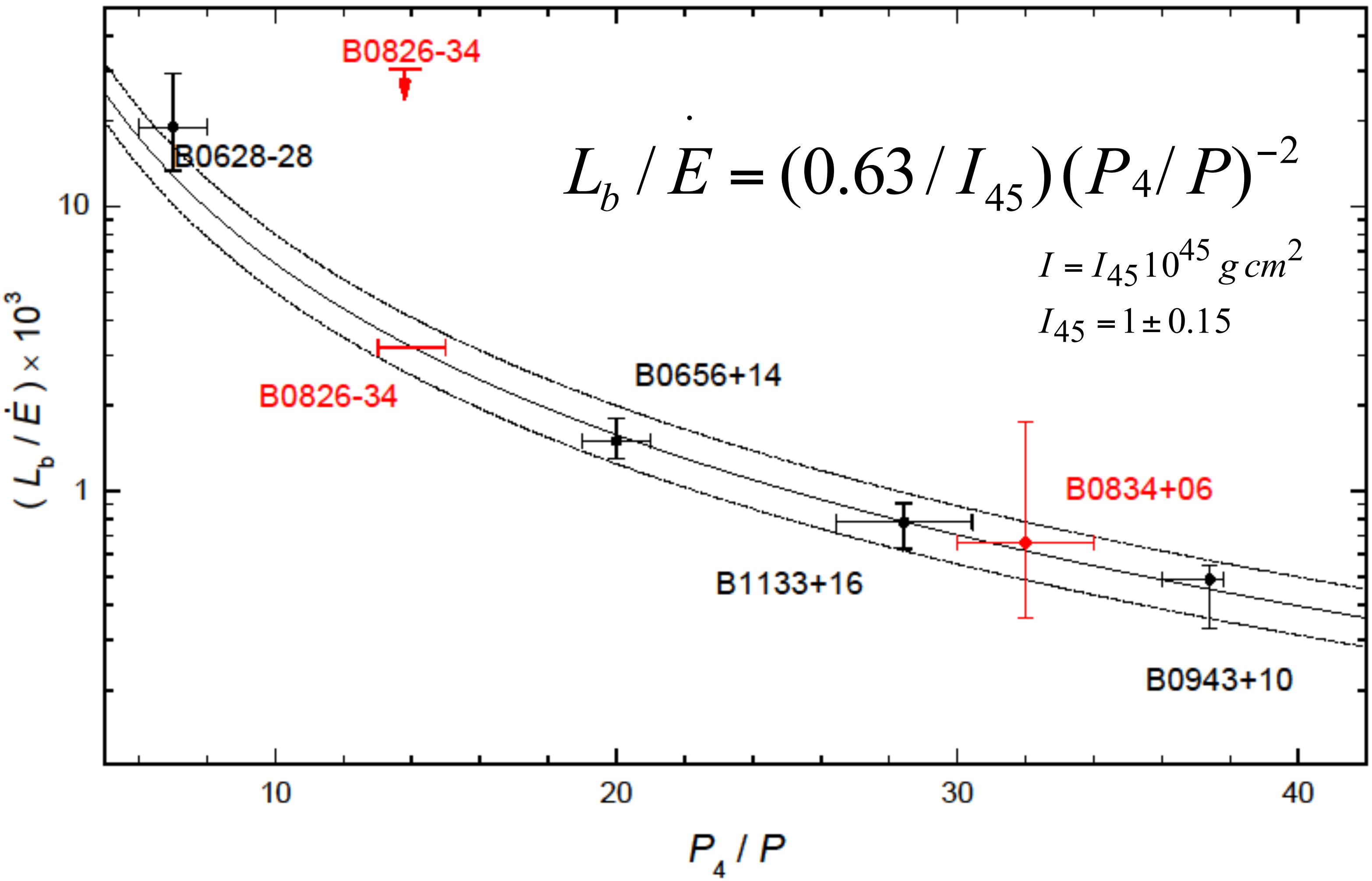
B0826-34
B0628-28
$L_b / \dot{E} = (0.63 / I_{45})(P_4 / P)^{-2}$
$I = I_{45} 10^{45}\, g\, cm^2$
$I_{45} = 1 \pm 0.15$
B0656+14
B0826-34
B0834+06
B1133+16
B0943+10
$(L_b / \dot{E}) \times 10^3$
P_4 / P
10
1
10
20
30
40

PSR J0108-1431

$$P = 0.8\,\mathrm{s},\ \dot{P}_{-15} = 0.08$$

$$A_{pc} \approx 8.2\times10^4\,\mathrm{m}^2$$

$$A_{\mathrm{BB}} \approx 50\,\mathrm{m}^2$$

$$A_{pc} \approx 1600\,A_{\mathrm{BB}}$$

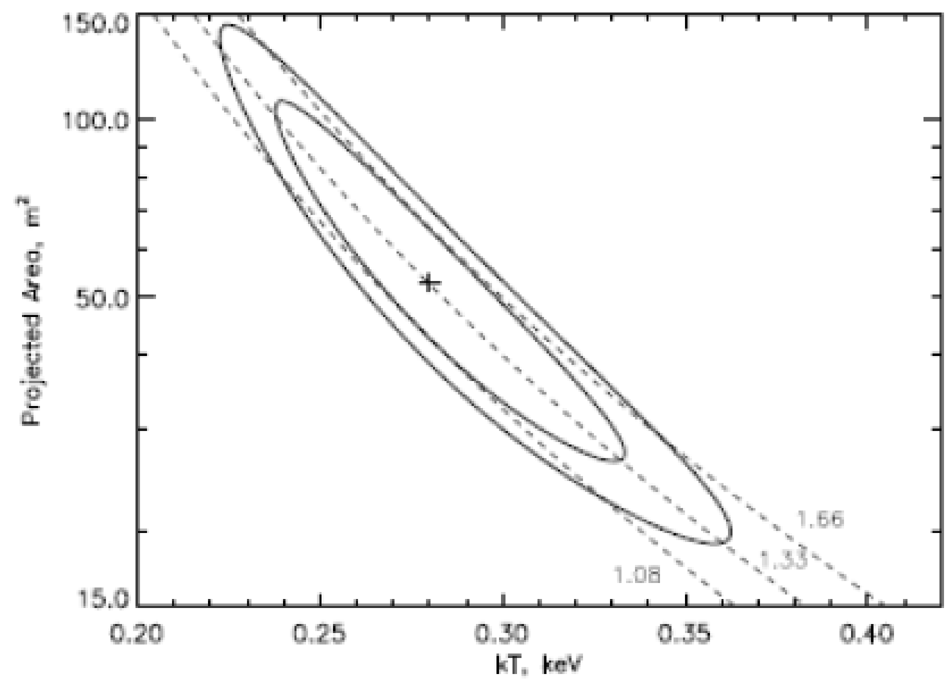

Confidence contours (68% and 90%) for the absorbed BB model with fixed NH = 7.3×10^{19} cm^{-2}. The BB normalization is expressed in terms of projected emitting area, in units of m^2 for d = 130 pc. The dashed lines are the lines of constant bolometric luminosity, in units of 10^{28} ergs s^{-1}, assuming d = 130 pc. (Pavlov, Kargaltsev, Wong & Garmire, ApJ, 691, 458, 2009)

Polar cap radius and hot spot surface area

Locus of the open magnetic field lines

$$r_{pc} = 1.45\times 10^{4} P^{-0.5}\ cm$$

Canonical radius for dipolar field lines at the NS surface

$$r_p = (B_s / B_d)^{-0.5} r_{pc}$$

Actual value for non-dipolar surface field

$$\boxed{B_s = B_d (A_p / A_{pc})}$$

B_s **Actual field**

B_d **Dipolar field**

$$A_p = \pi r_p^2 / b$$

Hot spot

Surface area

$$A_{pc} = \pi r_{pc}^2$$

conventional

Hot spot area should be much smaller than the canonical one !

In many cases the hot spot is really much smaller than the conventional PC


FEBRUARY 1 - 7, 2009
Thirty Years of Magnetars: New Frontiers

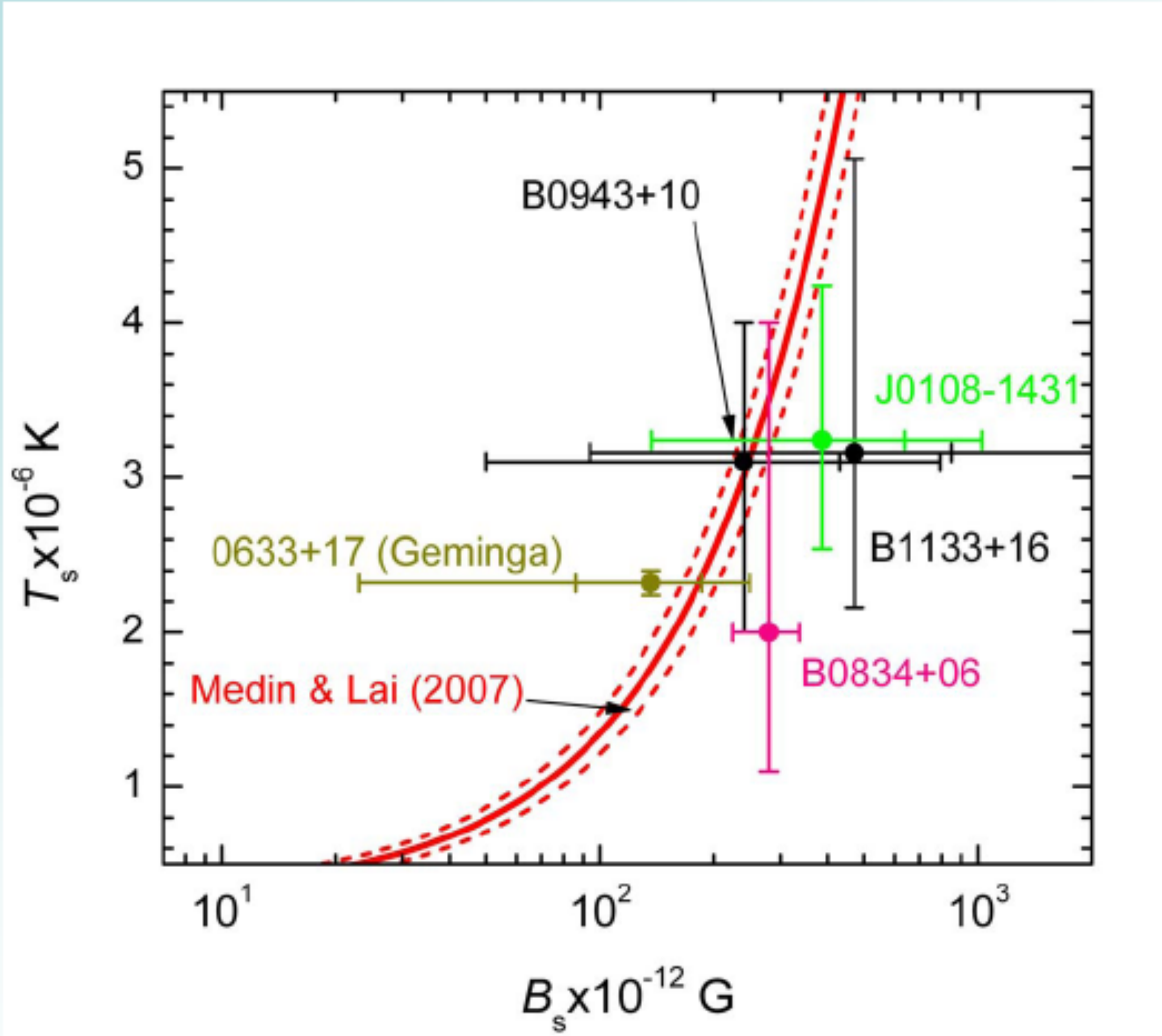
B0943+10
J0108-1431
B1133+16
0633+17 (Geminga)
B0834+06
Medin & Lai (2007)
T_sx10^{-6} K
B_sx10^{-12} G

$$B_s = B_d(A_p / A_{pc})$$

Pulsars are fast rotating and strongly magnetized Neutron Stars (NS)

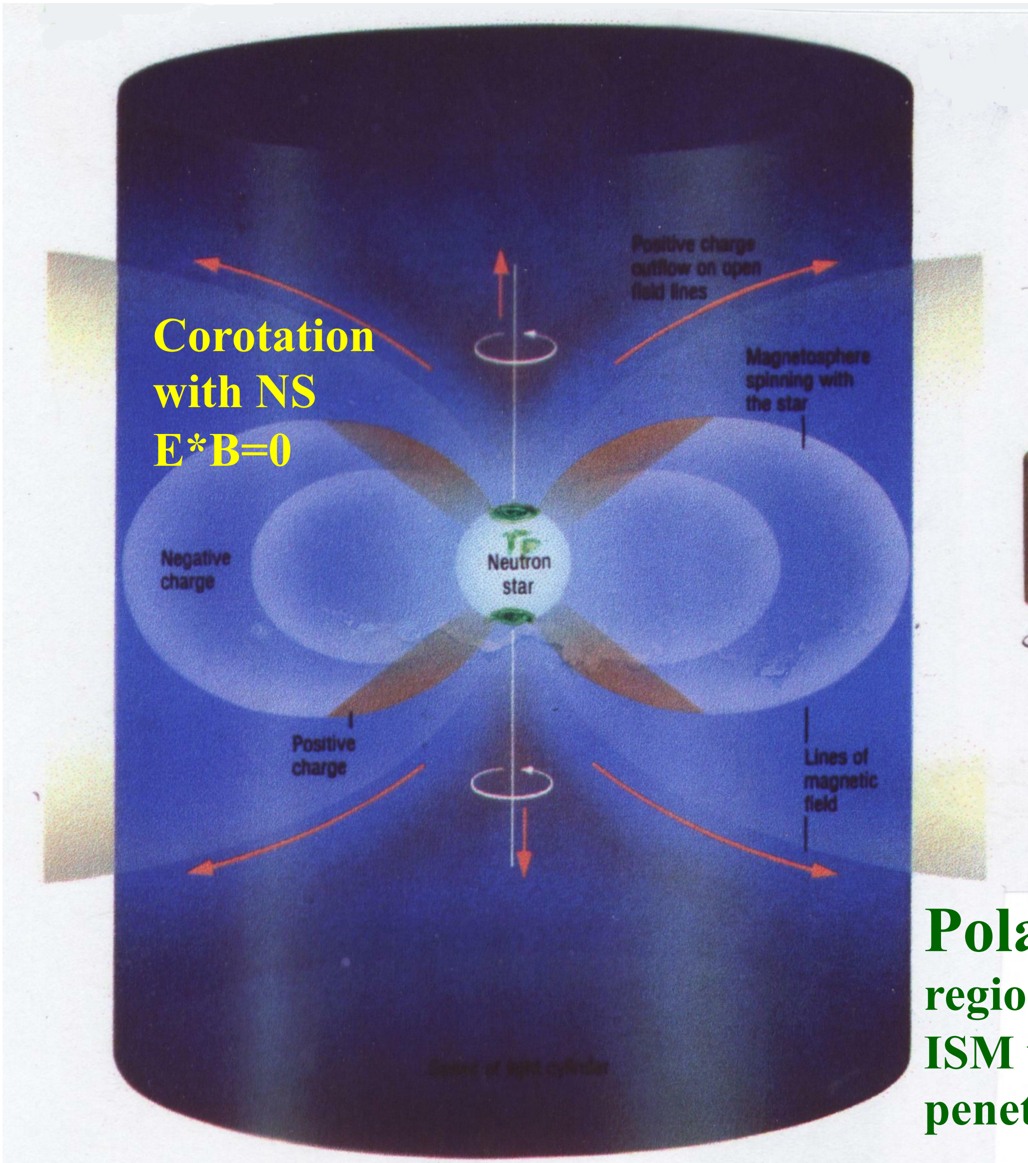

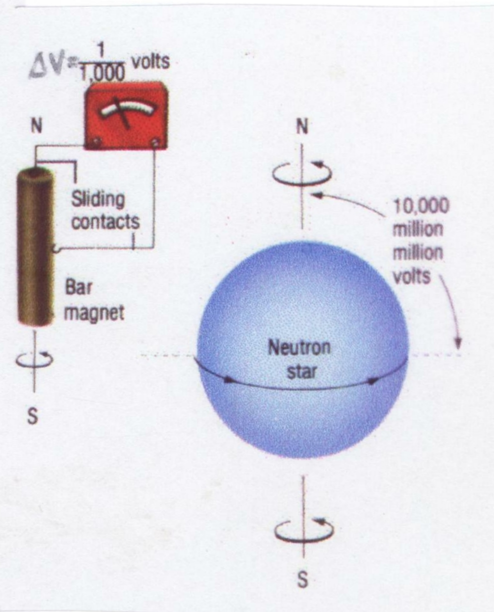

Polar Cap (PC)

region of NS surface connected to ISM via open magnetic field lines penetrating the Light Cylinder

Charged particles will leave through LC due to inertia and create charge depletion just above the PC. If this charge cannot be re-supplied by the PC surface (strong binding) then huge accelerating potential drop V~10^{12} V will occur along the open magnetic field lines close to the PC surface.

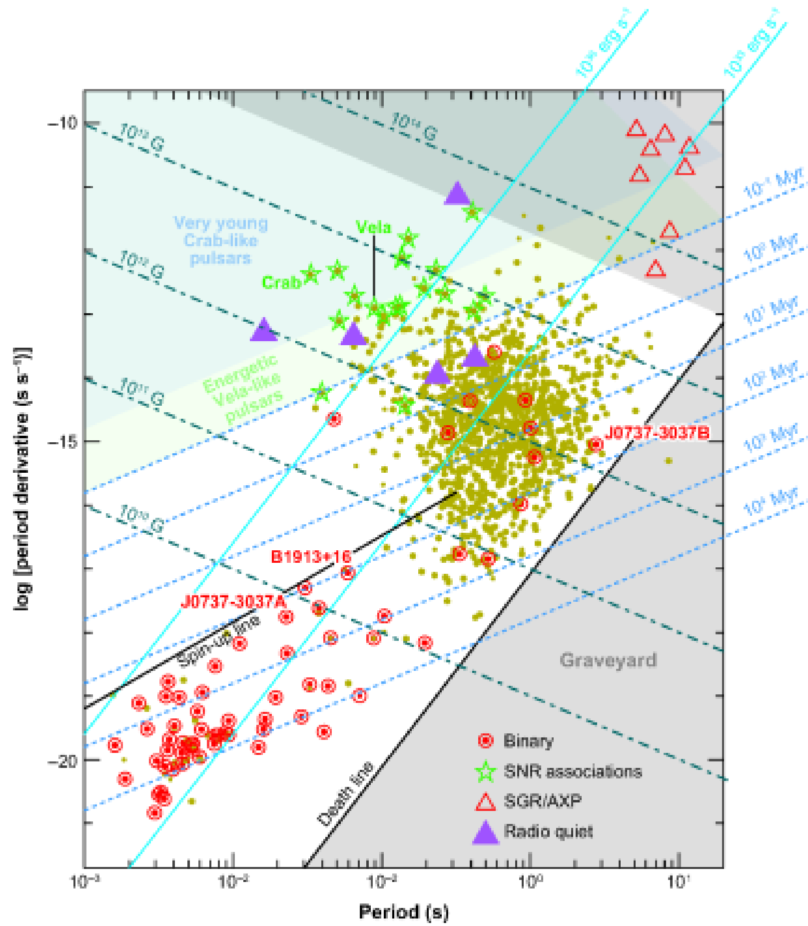
log [period derivative (s s⁻¹)]
Period (s)
Very young
Crab-like
pulsars
Energetic
Vela-like
pulsars
Crab
Vela
B1913+16
J0737-3037A
J0737-3037B
Spin-up line
Death line
Graveyard
Binary
SNR associations
SGR/AXP
Radio quiet

$$\rho_{GJ} = \frac{\Omega \cdot B_s}{2\pi c} = \frac{B_s}{cP} = \frac{bB_d}{cP}$$

$$\Delta\rho = \eta\rho_{GJ} = (1 - \rho_i / \rho_{GJ})\rho_{GJ} = \rho_{GJ} - \rho_i$$

$$\boxed{\frac{d^2 V_{\|}}{dz^2} = -4\pi\Delta\rho} \quad \frac{dV_{\|}(z=h)}{dz} = 0 \quad \frac{dV_{\|}(z=0)}{dz} = E_{\max}$$

$$E_{\|}(z) = \eta\left(\frac{4\pi}{cP_1}\right)B_s(h-z)$$

$$\boxed{\Delta V_{\|} = \int_0^z E(z)dz = \eta\frac{2\pi}{cP_1}B_s h^2}$$

$$h = l_{ph} \qquad \hbar\omega > 2mc^2$$

$$\Delta E_{\|} = \left(\eta\pi / cP\right) B_s h$$

$$\alpha = \frac{\Delta E_{\perp}}{\Delta E_{\|}}$$

$$v_d = c\frac{\Delta E_{\perp}}{B_s} = \pi\alpha\eta\, h / P$$

$$P_4 = \frac{2\pi r_p}{v_d}$$

$$\frac{P_4}{P} = 2\frac{r_p}{\alpha\eta h}$$